Eur Radiol (2018) 28:2058–2067
https://doi.org/10.1007/s00330-017-5146-8

GASTROINTESTINAL

Can CT-based radiomics signature predict *KRAS/NRAS/BRAF* mutations in colorectal cancer?

Lei Yang[1,2] · Di Dong[2,3,4] · Mengjie Fang[2,3] · Yongbei Zhu[2] · Yali Zang[2] · Zhenyu Liu[2] · Hongmei Zhang[1] · Jianming Ying[5] · Xinming Zhao[1] · Jie Tian[2,3,6]

Received: 8 August 2017 / Revised: 13 October 2017 / Accepted: 18 October 2017 / Published online: 15 January 2018

Abstract

Objectives To investigate whether CT-based radiomics signature can predict *KRAS/NRAS/BRAF* mutations in colorectal cancer (CRC).

Methods This retrospective study consisted of a primary cohort (n = 61) and a validation cohort (n = 56) with pathologically confirmed CRC. Patients underwent *KRAS/NRAS/BRAF* mutation tests and contrast-enhanced CT before treatment. A total of 346 radiomics features were extracted from portal venous-phase CT images of the entire primary tumour. Associations between the genetic mutations and clinical background, tumour staging, and histological differentiation were assessed using univariate analysis. RELIEFF and support vector machine methods were performed to select key features and build a radiomics signature.

Results The radiomics signature was significantly associated with *KRAS/NRAS/BRAF* mutations ($P < 0.001$). The area under the curve, sensitivity, and specificity for predicting *KRAS/NRAS/BRAF* mutations were 0.869, 0.757, and 0.833 in the primary cohort, respectively, while they were 0.829, 0.686, and 0.857 in the validation cohort, respectively. Clinical background, tumour staging, and histological differentiation were not associated with *KRAS/NRAS/BRAF* mutations in both cohorts (P>0.05).

Conclusions The proposed CT-based radiomics signature is associated with *KRAS/NRAS/BRAF* mutations. CT may be useful for analysis of tumour genotype in CRC and thus helpful to determine therapeutic strategies.

Key Points

- *Key features were extracted from CT images of the primary colorectal tumour.*
- *The proposed radiomics signature was significantly associated with KRAS/NRAS/BRAF mutations.*
- *In the primary cohort, the proposed radiomics signature predicted mutations.*
- *Clinical background, tumour staging, and histological differentiation were unable to predict mutations.*

Lei Yang and Mengjie Fang contributed equally to this work.

Electronic supplementary material The online version of this article (https://doi.org/10.1007/s00330-017-5146-8) contains supplementary material, which is available to authorized users.

✉ Di Dong
di.dong@ia.ac.cn

✉ Xinming Zhao
xinmingzh@sina.com

✉ Jie Tian
jie.tian@ia.ac.cn

[1] Department of Diagnostic Radiology, National Cancer Center/Cancer Hospital, Chinese Academy of Medical Sciences and Peking Union Medical College, No. 17, Pan Jia Yuan Nan-li, PO Box 2258, Beijing 100021, China

[2] CAS Key Laboratory of Molecular Imaging, Institute of Automation, Chinese Academy of Sciences, Beijing 100190, China

[3] University of Chinese Academy of Sciences, Beijing 100190, China

[4] Beijing Key Lab of Molecular Imaging, Beijing 100190, China

[5] Department of Pathology, National Cancer Center/Cancer Hospital, Chinese Academy of Medical Sciences and Peking Union Medical College, Beijing 100021, China

[6] The State Key Laboratory of Management and Control for Complex Systems, Institute of Automation, Chinese Academy of Sciences, Beijing 100190, China

Keywords Colorectal neoplasms · Adenocarcinoma · Mutation · Diagnostic imaging · ROC curve

Abbreviations and Acronyms

AFP	Alpha fetoprotein
AUC	Area under curve
CA199	Carbohydrate antigen 199
CA242	Carbohydrate antigen 242
CA724	Carbohydrate antigen 724
CEA	Carcinoembryonic antigen
CI	Confidence interval
CRC	Colorectal cancer
CT	Computed tomography
EGFR	Epidermal growth factor receptor
^{18}F-FDG PET/CT	Positron emission tomography/computerd tomography with ^{18}F-fluorodexyglucose
FFPE	Formalin-fixed paraffin- embedded
GLCM	Gray-level co-occurrence matrix
GLRLM	Gray-level run-length matrix
ICCs	Intra-/inter-class correlation coefficients
NCCN	Nationgal comprehensive cancer network
NGS	Next-generation sequencing
OR	Odds ratio
PACS	Picture archiving and communication system
ROC	Receiver operating characteristic
SUV	Standardized uptake value
TPS	Tissue polypeptide specific antigen
3D	Three-dimensional

Introduction

Treatments for patients with colorectal cancer have undergone significant advances during the past decades [1, 2]. Recently, advances in therapeutic strategies are playing a crucial role in the survival improvement [3, 4]. Genetic profiling of tumours is a powerful tool that allows personalized treatment through the development of targeted therapies [5]. Since 2016, the National Comprehensive Cancer Network (NCCN) guidelines have been recommending that all patients with suspected or proven metastatic colorectal cancer should have tumour tissue genotyped for *KRAS/NRAS/BRAF* mutations because either of these mutations predicts a lack of response to cetuximab and panitumumab, which are anti-epidermal growth factor receptor (EGFR) monoclonal antibodies [6–9]. Therefore, at pre-treatment or during treatment, identification of *KRAS/NRAS/BRAF* mutation status is crucial to predict the therapeutic effect and determine individual therapeutic strategies for patients with colorectal cancer. The pathologic mutation test for genetic status in colorectal cancer is the gold standard in clinical practice. However, archival tissue may not represent genotypic changes that have occurred since the tissue was taken, especially after multiple lines of treatment, and archival samples may be limited by intratumoral heterogeneity. Thus, the development of a method, which can be noninvasive, conveniently repeatable and may reflect intratumoral heterogeneity to help identify genetic mutation status, is of significance to provide an adjunct to histologic assessment in real time. Analysis of circulating DNA could be a noninvasive method for genotype analysis in colorectal cancer [10]. However, the possibility that insufficient quantity of DNA was released into circulation to enable detection may be a shortcoming for this approach. Imaging examination could display the whole tumour and may have the potential to supplement genotype analysis.

Since computed tomography (CT) is recommended by the NCCN guidelines as the preferred imaging examination for colorectal cancer in clinical practice, we chose CT-based image features for analysis in the current research. Several previous studies have used positron emission tomography/CT with ^{18}F-fluorodeoxyglucose (^{18}F-FDG PET/CT) or/and CT-based texture to assess the associations with genetic mutations (*KRAS*, *KRAS/BRAF*, or *KRAS/NRAS*) in colorectal cancer, metastatic colorectal cancer, or rectal cancer [11–17], but with conflicting results. Additionally, these studies analysed only one or two *KRAS/NRAS/BRAF* genes and lacked validation. Otherwise, NCCN guidelines (version 1.2017) recommended that PET/CT should only be used to evaluate an equivocal finding on a CT or in patients with strong contraindications to CT or in patients with potentially surgically curable M1 disease. Therefore, we just used CT, included three genes (*KRAS/NRAS/BRAF*), and our study groups consisted of a primary cohort and a validation cohort to investigate whether a CT-based signature can provide genetic mutation information in addition to routine diagnosis.

Radiomics is an emerging technique that converts medical images into a high-dimensional minable feature space and uses data mining for cancer diagnosis and prognosis [18–21]. The combined analysis of a panel of multiple features, which are usually applied as radiomics signatures, has been used in the prediction or prognosis of colorectal cancer, head and neck cancer, and lung cancer [22–24]. To the best of our knowledge, there is no research on whether a CT-based radiomics signature is associated with *KRAS/NRAS/BRAF* mutation status in colorectal cancer. Therefore, the aim of the study was to investigate whether a CT-based radiomics signature could predict *KRAS/NRAS/BRAF* mutations.

Materials and Methods

Patients

Estimation of sample size is described in Supplementary Information 1.

This study was approved by the medical ethics committee of our institution. For this retrospective study, the requirement of informed consent was waived. A total of 117 patients were identified for analysis. They were all pathologically confirmed colorectal cancer, took *KRAS/NRAS/BRAF* mutation tests and underwent contrast-enhanced CT with a reconstructed slice thickness of 1.25 mm before treatment from November 2013 to May 2017 (Supplementary Information 2 and 5.1).

The patients were divided into two cohorts according to chronological order: a primary cohort (n = 61, November 2013–July 2015) and a validation cohort (n = 57, August 2015–May 2017). The primary cohort consisted of 41 men and 20 women (mean age, 54.38 years; age range, 25–76 years), while the validation cohort comprised 34 men and 22 women (mean age, 53.16 years; age range, 25–73 years).

Clinical and pathologic characteristics

Clinical and pathologic characteristics consisted of age, gender, tumour size, tumour location, differentiation degree of tumour, TNM stage (tumour, node, and metastases), smoking history, hypertension history, family history of cancer, and diabetes history. Laboratory analysis included carcinoembryonic antigen (CEA), carbohydrate antigen 242 (CA242), alpha fetoprotein (AFP), carbohydrate antigen 724 (CA724), carbohydrate antigen 199 (CA199), and tissue polypeptide specific antigen (TPS), which had threshold values of 5 ng/mL, 20 U/mL, 7 ng/mL, 9.8 U/mL, 37 U/mL, and 55 mU/mL, respectively, according to laboratory testing instructions (Roche, Basel, Switzerland).

KRAS/NRAS/BRAF mutation analysis

DNA was extracted from formalin-fixed paraffin-embedded (FFPE) tumour sections using the QIAamp DNA FFPE Tissue Kit (Qiagen). Mutations of *KRAS* (exons 2, 3, and 4), *NRAS* (exons 2, 3, and 4), and *BRAF* (V600E) were analysed by a next-generation sequencing (NGS) method.

Image acquisition and segmentation

All patients underwent contrast-enhanced abdominal and pelvic CT using one of two 64-detector row spiral CT systems. All portal venous-phase CT images were retrieved from a picture archiving and communication system (PACS; CAREstream Medical Ltd.) for image segmentation and analysis. The CT image acquisition, segmentation and intra-/inter-reader agreement evaluation are described in Supplementary Information 3.

Radiomics feature extraction and analysis

A total of 346 3D features from primary tumours were extracted, which were divided into four groups: (I) shape features, (II) grey-level histogram features, (III) grey-level co-occurrence matrix (GLCM) features, and (IV) grey-level run-length matrix (GLRLM) features (Fig. 1). The radiomics feature extraction methodology is described in Supplementary Information 4. Feature selection and modelling were based on the primary cohort. The processes of this section are listed in Table 1.

Firstly, based on the different groups of the independent segmentations of 30 patients, the intra-/inter-class correlation

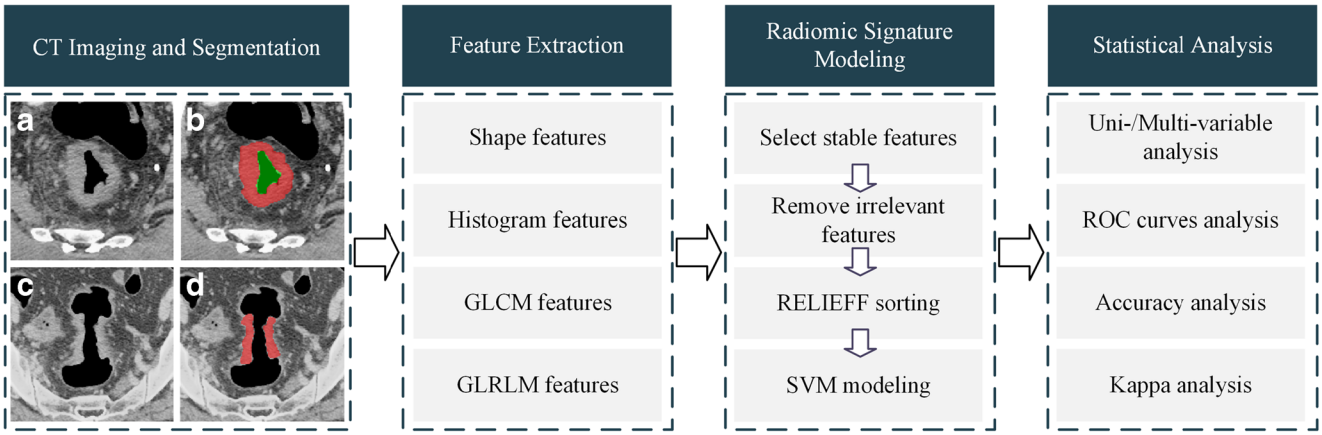

Fig. 1 Radiomics modelling and analysis workflow with two examples of CT images and tumour segmentation. (**a**, **b**) One patient with rectal cancer, male, 55 years old. The *red area* in (**b**) represents the maximum cross-sectional area of the tumour on this image; the *green area* in (**b**) is excluded, which is the air area in the tumour centre. (**c**, **d**) Another patient with sigmoid colon cancer, female, 53 years old. The *red area* in (**d**) represents the maximum cross-sectional area of the tumour on this image

Table 1 Post-processing workflow in this study

Step	Description	Software	Processing time
Image filtration	Multiple-filtering to implement image smoothing and image difference.	MATLAB with in-house software	a few seconds
Feature generation	Extracting a total of 346 3D features belonging to 4 groups	MATLAB with in-house software	about one minute
Reproducibility analysis	Estimating the intra-/inter-reader agreement of features	R with "psych" package	a few seconds
Univariate analysis	Evaluating if there are potential associations between features and genetic mutations	R with "stats" package	a few seconds
Feature ranking	Finding the features having the top powerful predictive ability in each feature set	MATLAB with FSLib toolbox	a few seconds
Signature modeling	Building and selecting the SVM models via multiple 10-fold cross validation	MATLAB with in-house software	a few minutes

coefficients (ICCs) were used to estimate the robustness of the features [25]. The stable features with ICCs of > 0.8 remained.

Secondly, univariate analysis was performed for each feature. Features with P values < 0.1 were considered to be associated with genetic mutations [26] and were selected into the following process.

Thirdly, five feature sets were established for model building. The five feature sets included: (I) shape feature set, (II) grey-level histogram feature set, (III) GLCM feature set, (IV) GLRLM feature set, and (V) the overall feature set. The RELIEFF algorithm was used to select features on each feature set [27]. To avoid model overfitting, the rule of thumb is that the number of predictors should remain within 1/10–1/3 of the sample size in each group of the primary cohort. Therefore, the potential feature set was limited to no more than three for prediction in this study (37 mutation-positive patients and 24 mutation-negative patients in the primary cohort).

Finally, we used a support vector machine (SVM) algorithm for radiomics signature modelling on each feature set. A sequential minimal optimization algorithm was used to train the model [28], a radial basis function was used as the kernel function, and a 1000 times 10-fold cross-validation was used in the training process to prevent overfitting and to select the model with the best performance.

The process of radiomics feature extraction and analysis was performed in MATLAB 2014a (MathWorks), including the Feature Selection Library (FSLib) toolbox [29].

Statistics

Univariate analysis was used to assess the relationship between the genetic mutation status and the characteristics of patients, including radiomics features and clinical characteristics. The differences in variables between the patients in different groups were assessed using t-test or the Mann-Whitney U test for continuous variables and the chi-square test for categorical variables. The radiomics signature was analysed using the receiver operating characteristic (ROC) curve. An odds ratio (OR) was used to indicate the degree of risk when the classification result was 1. The statistical power of the chi-square test in this study was estimated using the STPLAN software. Kappa tests and the Bland-Altman plots were used to determine intra-/inter-reader agreement. The 95% confidence interval (CI) for the limits of agreement was also calculated. Statistical analysis was conducted with R software (version 3.0.1; http://www.Rproject.org) and MATLAB. A two-sided P value of < 0.05 was used as the criterion to indicate a statistically significant difference.

Results

Clinical and pathologic characteristics

Based on the results of *KRAS/NRAS/BRAF* mutations, the patients were classified into two groups: the mutated group (either mutated *KRAS*, *NRAS*, or *BRAF*) and the wild-type group (nonmutated *KRAS*, *NRAS*, and *BRAF*). The distribution of genetic mutations in the primary and validation cohorts are shown in Table 2. There were no demographic differences in terms of age, gender, and genetic mutation status between the primary and validation cohorts (Supplementary Information 6.1).

Patient and tumour characteristics in the primary and validation cohorts are listed in Table 3. There were no significant differences between the mutated group and the wild-type group in either cohort in terms of tumour size, tumour location, histologic type, TNM stage (including T, N, and M categories), smoking history, hypertension history, family history of cancer, and diabetes history. There were significant differences in gender and age between the two groups in the primary cohort (P values of < 0.05), but they were not confirmed in the validation cohort. There were also no significant differences between the mutated group and the wild-type group in both cohorts in terms of CEA, CA242, AFP, CA724, CA199, and TPS levels (Supplementary Information 6.2).

Table 2 Distribution of genetic mutations in the primary and validation cohorts

Genetic mutation status	No. of patients	
	Primary cohort (n=61)	Validation cohort (n=56)
Mutated group (either mutated *KRAS* or *NRAS* or *BRAF*)	37 (60.66%)	35 (62.50%)
Mutated *KRAS* only	30 (49.18%)	27 (48.21%)
Mutated *NRAS* only	4 (6.56%)	4 (7.14%)
Mutated *BRAF* only	2 (3.28%)	4 (7.14%)
Mutated *KRAS*/*BRAF* simultaneous	1 (1.64%)	
Wild-type group (nonmutated *KRAS* and *NRAS* and *BRAF*)	24 (39.34%)	21 (37.50%)

Note: n, number.

Feature selection and radiomics signature modelling

After assessing the reproducibility, 296 robust texture features remained, with ICCs of > 0.8. Meanwhile, 56 of the 296 features showed potential predictive abilities in the initial single-factor analysis. Followed by the establishment of the five feature sets, we used the RELIEFF algorithm to sort the features and selected the three top features in each feature set as the input variables for SVM models. The results of the feature selection and the 1000 times 10-fold cross-validation are shown in Table 4. Having the best predictive performance, the SVM trained based on the overall feature set was selected. The descriptions and performances of the model's input features are presented in Table 5. Since each feature can be thought of as one dimension, a three-dimensional feature space was constructed by the three selected features. The patients were projected into the feature space as a point and the SVM model hyperplane, i.e. the optimal threshold, was also described. The illustrations of the hyperplane and the distribution of patients in the feature space are shown in Fig. 2. The optimal hyperplane was estimated based on the rule that the prediction power of the model should be maximum in the primary cohort while ensuring its generalization performance. The radiomics signature scores of patients, which were the numeric results calculated via the SVM model, are described in Table 5.

There were excellent intra-/inter-reader agreement for our SVM model with the kappa values of 0.867 and 0.800, respectively. The Bland-Altman plots are shown in Supplementary Information 5.3.

Validation of radiomics signature

Calculated by the STPLAN software, the power of validation was 0.996 under a given significance level ($P = 0.05$).

The SVM model for differentiating the mutated group from the wild-type group showed an accuracy of 0.787 (95% CI, 0.669–0.871; sensitivity, 0.757; specificity, 0.833) in the primary cohort and 0.750 (95% CI, 0.623–0.845; sensitivity, 0.686; specificity, 0.857) in the validation cohort. The value of radiomics signature was highly correlated with genetic mutations (primary cohort: $P < 0.001$; OR, 22.19 [95% CI, 5.02–98.08]; validation cohort: $P < 0.001$; OR, 11.18 [95% CI, 2.88–43.36]).

In the ROC analysis, the radiomics signature yielded an area under curve (AUC) of 0.869 (95% CI, 0.780–0.958) in the primary cohort and 0.829 (95% CI, 0.718–0.939) in the validation cohort, shown in Fig. 3(a). The radiomics signature scores for each patient in the primary and validation cohorts with regard to the mutated and wild-type groups are depicted in Fig. 3(b).

Gender, age, and radiomics signature were used as input variables for multivariate logistic regression analysis. The result showed that only the radiomics signature was the independent predictor.

Discussion

The proposed CT-based radiomics signature is associated with *KRAS/NRAS/BRAF* mutations. It shows preferable AUC and specificity for predicting *KRAS/NRAS/BRAF* mutations, while it presents a relatively low sensitivity, especially in the validation cohort. The radiomics signature incorporates three radiomics features. Clinical background, tumour staging, and histological differentiation are not associated with *KRAS/NRAS/BRAF* mutations in both cohorts. The results indicate that CT may be useful for predicting *KRAS/NRAS/BRAF* status of patients with colorectal cancer and thus have the potential to aid in determination of therapeutic strategies.

Previous studies tried to investigate the relationship between image characteristics and genetic mutations (*KRAS*, *KRAS/BRAF*, or *KRAS/NRAS*) in colorectal cancer, metastatic colorectal cancer, or rectal cancer [11–17], and the most used imaging technique was ^{18}F-FDG PET/CT. Kawada et al. concluded that ^{18}F-FDG PET/CT may be useful for predicting the

Table 3 Patient and tumor characteristics in the primary and validation cohorts

Characteristics	Primary cohort		*P*	Validation cohort		*P*
	Wild-type group	Mutated group		Wild-type group	Mutated group	
Age, years (Mean ± SD)	50.08±11.81	57.16±10.24	0.039*	52.9±10.21	53.31±10.02	0.806
Gender, n (%)			0.015*			0.672
Male	21(87.50%)	20(54.05%)		14(66.67%)	20(57.14%)	
Female	3(12.50%)	17(45.95%)		7(33.33%)	15(42.86%)	
Tumor size, cm (Mean ± SD)	2.10±0.85	1.80±0.76	0.168	1.79±1.15	2.01±0.65	0.435
Tumor location, n (%)			0.665			0.112
Ascending colon	1(4.17%)	5(13.51%)		1(4.76%)	8(22.86%)	
Transverse colon	1(4.18%)	1(2.70%)		0(0.00%)	2(5.71%)	
Descending colon	3(12.50%)	2(5.41%)		0(0.00%)	3(8.57%)	
Sigmoid colon	3(12.51%)	8(21.62%)		3(14.28%)	2(5.71%)	
Rectum	15(62.50%)	20(54.05%)		15(71.43%)	20(57.14%)	
Cecum	1(4.17%)	1(2.70%)		1(4.76%)	0(0.00%)	
Histologic grade, n (%)			0.185			0.260
Well	0(0.00%)	0(0.00%)		3(14.28%)	2(5.71%)	
Moderate	12(50.00%)	26(70.27%)		14(66.67%)	20(57.14%)	
Poor	12(50.00%)	11(29.73%)		4(19.05%)	13(37.14%)	
TNM stage, n (%)			0.892			0.609
I	0(0.00%)	0(0.00%)		1(4.76%)	1(2.86%)	
II	2(8.33%)	2(5.41%)		3(14.28%)	6(17.14%)	
III	14(58.33%)	23(62.16%)		10(47.62%)	11(31.43%)	
IV	8(33.33%)	12(32.43%)		7(33.33%)	17(48.57%)	
T category, n (%)			0.962			0.795
T1	0(0.00%)	0(0.00%)		0(0.00%)	0(0.00%)	
T2	0(0.00%)	0(0.00%)		1(4.76%)	1(2.86%)	
T3	12(50.00%)	20(54.05%)		12(57.14%)	23(65.71%)	
T4	12(50.00%)	17(45.95%)		8(38.10%)	11(31.43%)	
N category, n (%)			0.975			0.426
N0	2(8.33%)	3(8.11%)		4(19.05%)	10(28.57%)	
N1, N2	22(91.67%)	34(91.89%)		17(80.95%)	25(71.43%)	
M category, n (%)			0.942			0.265
M0	16(66.67%)	25(67.57%)		14(66.67%)	18(51.43%)	
M1	8(33.33%)	12(32.43%)		7(33.33%)	17(48.57%)	
Smoking, n (%)			0.291			0.833
No	13(54.17%)	25(67.57%)		12(57.14%)	21(60.00%)	
Yes	11(45.83%)	12(32.43%)		9(42.86%)	14(40.00%)	
Hypertension, n (%)			0.353			0.824
No	17(70.83%)	30(81.08%)		19(90.48%)	31(88.57%)	
Yes	7(29.17%)	7(18.92%)		2(9.52%)	4(11.43%)	
Family history of cancer, n (%)			0.571			0.541
No	18(75.00%)	30(81.08%)		16(76.19%)	24(68.57%)	
Yes	6(25.00%)	7(18.92%)		5(23.81%)	11(31.43%)	
Diabetes, n (%)			0.255			0.434
No	22(91.67%)	30(81.08%)		18(85.71%)	27(77.14%)	
Yes	2(8.33%)	7(18.92%)		3(14.29%)	8(22.86%)	
Radiomic signature score, median (interquartile range)	-0.545 (-0.981~-0.2203)	0.744 (0.046~0.967)	<0.001*	-0.280 (-0.676~-0.160)	0.393 (-0.091~0.735)	<0.001*

Note: n, number; *P* value was derived from the univariable association analyses between each characteristic and genetic mutation status; tumor size was measured at the thickest part of the colorectal lesion vertical to the bowel wall on the cross-sectional image (Supplementary Information 5.2).

*, $P < 0.05$.

KRAS/BRAF mutations with an accuracy of 75%. The sensitivity and specificity were 74% and 75% when a maximum standardized uptake value (SUV_{max}) cut-off value of 13 was used, respectively [12]. Chen et al. showed that SUV_{max} and TW40% (40% of the SUV_{max}) were associated with *KRAS* mutations in colorectal cancer according to different location of primary tumours. The SUV_{max} value was statistically significant for predicting *KRAS* mutations in the subgroup of colon or sigmoid colon cancer with the accuracy, sensitivity, and specificity of 68.1%, 54.3%, and 81%, respectively, whereas TW40% was significantly higher in the *KRAS* mutant group in the subgroup of rectum or rectosigmoid junction cancer with the accuracy, sensitivity, and specificity of 71.4%, 80%, and 79.1%, respectively [15] Kawada et al. found that *KRAS* status could be predicted in metastatic colorectal cancer by ^{18}F-FDG PET/CT with the accuracy of 71.4%

Table 4. Results of the model selection process

Feature set	Selected features	Performance in 1000 times 10-fold validation			
		Accuracy (95% CI)	Sensitivity	Specificity	AUC (95% CI)
Shape	surface_area_to_volume_ratio maximum_radius volume	0.706(0.599-0.780)	0.685	0.734	0.760(0.682-0.820)
Histogram	3_fos_mean_absulute_deviation 2_fos_range 1_fos_skewness	0.676(0.580-0.766)	0.505	0.936	0.807(0.716-0.894)
GLCM	4_GLCM_maximum_probability 6_GLCM_energy 1_GLCM_inverse_variance	0.752(0.671-0.811)	0.679	0.872	0.842(0.757-0.897)
GLRLM	3_GLRLM_LGLRE 1_GLRLM_RP 7_GLRLM_RP	0.746(0.643-0.833)	0.669	0.854	0.834(0.703-0.912)
Overall	4_GLCM_maximum_probability 6_GLCM_energy 8_GLCM_sum_average	0.766(0.673-0.836)	0.701	0.858	0.860(0.797-0.928)

Note: CI, confidence interval; the number in the front of each feature name represents the kind of filter used before feature extraction; the three top features of the overall feature set were all the GLCM features; therefore, the third was removed before sorting the GLCM feature set to avoid the construction of a repeated model.

when using an SUV_{max} cut-off value of 6. The AUC, sensitivity, and specificity for predicting *KRAS* mutations were 0.7, 68%, and 74%, respectively [14]. Miles et al. found that multifunctional imaging parameters, which included ^{18}F-FDG uptake, CT texture, and blood flow measured by contrast-enhanced CT, were associated with *KRAS* mutation with the accuracy, true-positive rate, and false-positive rate were 90.1%, 82.4%, and 0% [13]. On the contrary, Krikelis et al. found that ^{18}F-FDG PET/CT SUV_{max} was not statistically significant correlated with *KRAS* mutation in Caucasian metastatic colorectal cancer [17]. Different from ^{18}F-FDG PET/CT, CT is the preferred imaging examination for colorectal cancer in clinical practice. CT-based quantitative metrics analysis, such as CT texture, has been used in the prediction of cancer [30]. In the field of genetic mutation prediction, CT texture has been used to be assessed the relationship with *KRAS* mutation in colorectal cancer [11]. The results showed that skewness was negatively associated with *KRAS* mutation. In our study, skewness also showed the potential predictive power. However, it did not remain in the final selection step

Table 5 Descriptions of the three selected features and their performances

Features	Filters	Primary cohort		*P*	Validation cohort		*P*
		Wild-type group	Mutated group		Wild-type group	Mutated group	
4_GLCM_maximum_probability	X_{LHH}	0.0362 ±0.0025	0.0379 ±0.0024	0.014*	0.0365 ±0.0020	0.0378 ±0.0021	0.029*
6_GLCM_energy	X_{HLH}	0.0162 ±0.0012	0.0169 ±0.0013	0.030*	0.0163 ±0.0010	0.0170 ±0.0016	0.042*
8_GLCM_sum_average	X_{HHH}	25.8407 ±0.0584	25.8787 ±0.0916	0.038*	25.8551 ±0.0649	25.8741 ±0.0802	0.491

Note: data are mean ± standard deviation; *P* value was derived from the univariable association analyses between each feature and genetic status.

*, $P < 0.05$.

X_{LHH}: The original image was filtered directionally with a low-pass filter along the *x* directions and with a high-pass filter along the *y* and *z* directions.
X_{HLH}: The original image was filtered directionally with a high-pass filter along the *x* and *z* directions and with a low-pass filter along the *y* direction.
X_{HHH}: The original image was filtered directionally with a high-pass filter along all three directions.

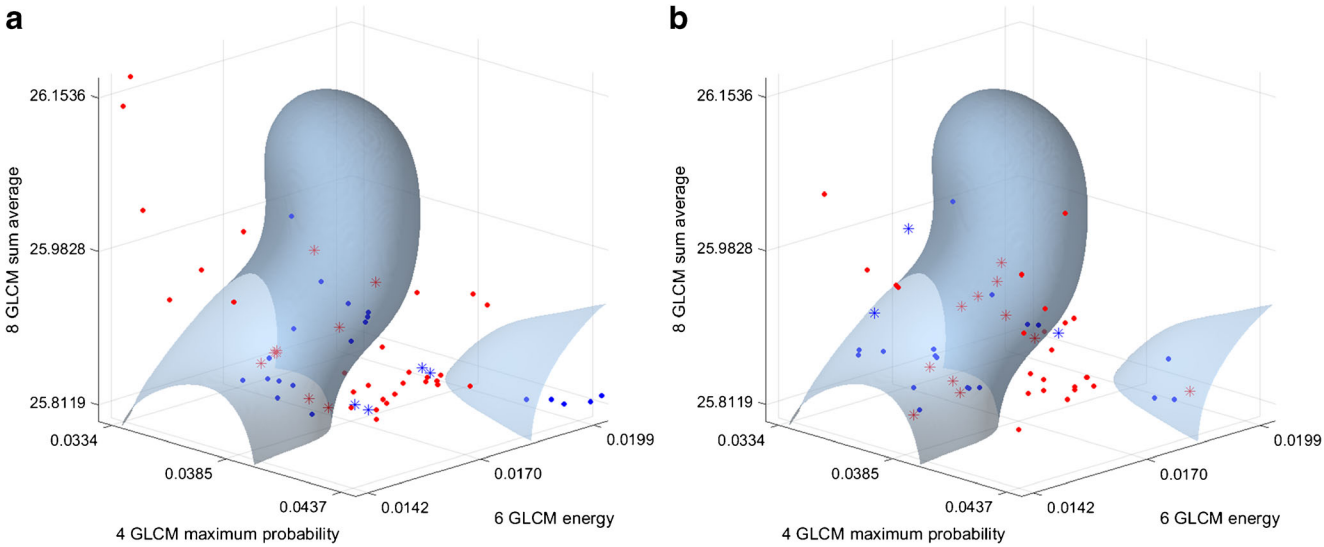

Fig. 2 The separation hyperplane of the SVM model, along with the patients in (**a**) the primary cohort and (**b**) the validation cohort. The *grey surface* represents the hyperplane. The points represent the patients (TN, *blue solid points*; TP, *red solid points*; FN, *red stars*; FP, *blue stars*)

because other selected radiomics features displayed better predictive abilities. The proposed CT-based radiomics signature incorporates three radiomics features. Clinical background, tumour staging and histological differentiation were not associated with *KRAS/NRAS/BRAF* mutations in both cohorts. The AUC, sensitivity, and specificity for predicting *KRAS/NRAS/BRAF* mutations were 0.869, 0.757, and 0.833 in the primary cohort, respectively, while they were 0.829, 0.686, and 0.857 in the validation cohort, respectively. It shows preferable AUC and specificity compared with other research. However, it presents a relatively low sensitivity, especially in the validation cohort. The improvement of sensitivity is needed for clinical use in the future.

As a preliminary study, it still has some limitations. Firstly, we just included a single team with an internal validation and specific machines/software. The reproducibility of our model under different imaging settings should be justified via more external validation in the

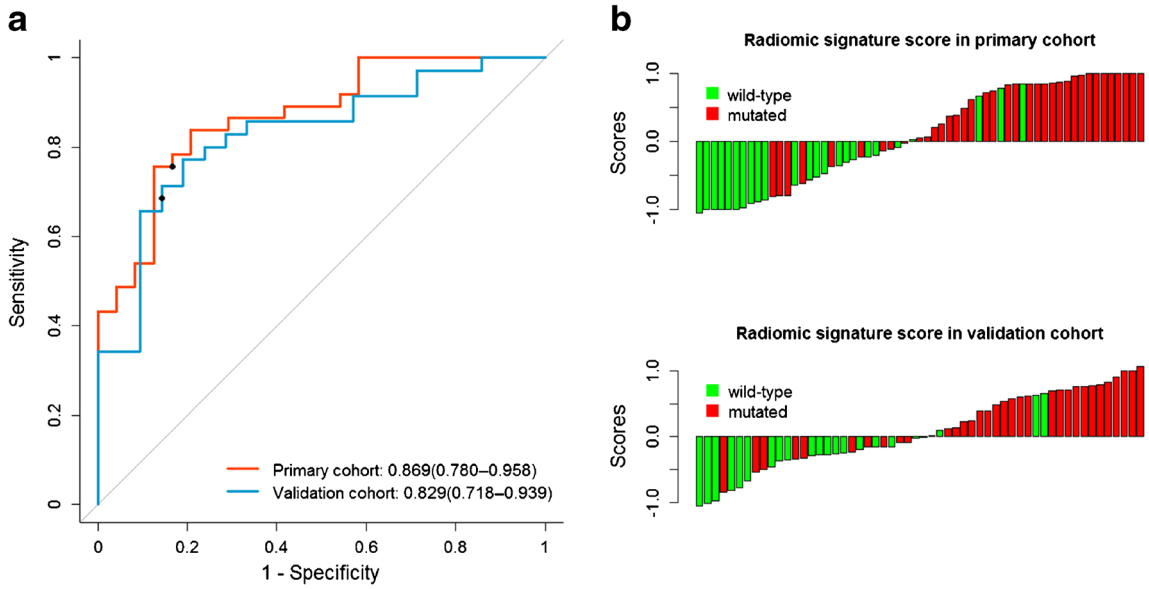

Fig. 3 The SVM performance of predicting *KRAS/NRAS/BRAF* mutations. (**a**) ROC curves and the AUC for the radiomics signature score. The *red line* and the *blue line* represent the ROC curves in the primary cohort and the validation cohort, respectively. The *solid dots* represent the optimal cut-off value (i.e., the SVM model hyperplane) for the discrimination calculated based on the primary cohort. (**b**) A radiomics signature score for every patient in each cohort. The *red marks* indicate the patients in the mutated group, while the *green marks* indicate the patients in the wild-type group.

future because different features are always affected by the reconstruction settings in varying degrees [31]. Secondly, the study included stages I, II, III, and IV of colorectal cancer patients, similar to other studies [12, 13]. Although it is reasonable to include all four stages of patients to analyse the relationship between radiomics features and genetic status, the better choice might be including only stage IV patients because there is less heterogeneity intratumorally in terms of *KRAS* mutations in stage IV colorectal cancer tumours [32]. Thirdly, it will be better for us to investigate whether the radiomics signature can predict the survival rates of anti-EGFR therapy in the future.

For the radiomics signature construction, 346 candidate features were reduced to three key features. Finally, the selected radiomics signature comprised 6_GLCM_energy, 4_GLCM_maximum_probability, and 8_GLCM_sum_average. In our previous work, we used a linear combination of features for lymph node prediction in colorectal cancer [18] and progression free survival prediction in advanced nasopharyngeal carcinoma [21]. The latent relation among genetic status, intratumor heterogeneity and radiological phenotype features is complex and maybe non-linear, and therefore, we combined the three selected features to a radiomics signature based on a machine learning method with the competence to recognize the deeper pattern. Machine learning is an advanced technology now widely used in medical diagnosis [33–35]. When applied to the problems of status classification, machine learning can be classified into two categories: one based on the statistical pattern and the other based on the neural network. While the artificial neural network, especially the deep convolutional neural network [33, 34], has achieved remarkable performances in many clinical medical applications with a large sample size, an SVM is a type of statistical classifier model based on structural risk minimization and has been used to solve a series of nonlinear problems with a small sample size. In this study, a SVM was used for radiomics signature modelling. For the predictive problem of genetic status, the proposed SVM-based radiomics signature achieved noticeable results in both primary and validation cohorts, making it a promising method to facilitate the prediction of *KRAS/NRAS/BRAF* mutations in patients with colorectal cancer for guiding targeted therapy.

In conclusion, the proposed CT-based radiomics signature is associated with *KRAS/NRAS/BRAF* mutations. CT may be useful for analysis of tumour genotype in CRC and thus helpful to determine therapeutic strategies.

Funding This study has received funding by the National Natural Science Foundation of China (grant numbers 81227901, 81771924, 61231004, 81501616, 81671851, 81527805, 81501549, 81671829 and 81671757), the National Key R&D Program of China (grant numbers 2017YFA0205200, 2017YFC1308700, 2017YFC1309100, and 2017YFC1308701), the Science and Technology Service Network Initiative of the Chinese Academy of Sciences (grant number KFJ-SW-STS-160), the Instrument Developing Project (grant number YZ201502), the Beijing Municipal Science and Technology Commission (grant number Z161100002616022), and the Youth Innovation Promotion Association CAS.

Compliance with ethical standards

Guarantor The scientific guarantor of this publication is Jie Tian.

Conflict of interest The authors of this manuscript declare no relationships with any companies, whose products or services may be related to the subject matter of the article.

Statistics and biometry No complex statistical methods were necessary for this paper.

Informed consent Written informed consent was waived in this study.

Ethical approval Institutional Review Board approval was obtained.

Methodology
- retrospective
- diagnostic experimental
- performed at one institution

References

1. van de Velde CJ, Boelens PG, Borras JM et al (2014) EURECCA colorectal: multidisciplinary management: European consensus conference colon & rectum. Eur J Cancer 50:1.e1–1.e34
2. Cremolini C, Loupakis F, Antoniotti C et al (2015) FOLFOXIRI plus bevacizumab versus FOLFIRI plus bevacizumab as first-line treatment of patients with metastatic colorectal cancer: updated overall survival and molecular subgroup analyses of the open-label, phase 3 TRIBE study. Lancet Oncol 16:1306–1315
3. Strickler JH, Wu C, Bekaii-Saab T (2017) Targeting BRAF in metastatic colorectal cancer: maximizing molecular approaches. Cancer Treat Rev 60:109–119
4. Sundar R, Hong DS, Kopetz S, Yap TA (2017) Targeting BRAF-mutant colorectal cancer: progress in combination strategies. Cancer Discov 7:558–560
5. De Roock W, Claes B, Bernasconi D et al (2010) Effects of KRAS, BRAF, NRAS, and PIK3CA mutations on the efficacy of cetuximab plus chemotherapy in chemotherapy-refractory metastatic colorectal cancer: a retrospective consortium analysis. Lancet Oncol 11:753–762
6. Van Cutsem E, Lenz HJ, Köhne CH et al (2015) Fluorouracil, leucovorin, and irinotecan plus cetuximab treatment and RAS mutations in colorectal cancer. J Clin Oncol 33:692–700
7. Peeters M, Oliner KS, Price TJ et al (2015) Analysis of KRAS/NRAS mutations in a phase III study of panitumumab with FOLFIRI compared with FOLFIRI alone as second-line treatment for metastatic colorectal cancer. Clin Cancer Res 21:5469–5479
8. Barras D, Missiaglia E, Wirapati P et al (2017) BRAF V600E mutant colorectal cancer subtypes based on gene expression. Clin Cancer Res 23:104–115

9. Douillard JY, Oliner KS, Siena S et al (2013) Panitumumab-FOLFOX4 treatment and RAS mutations in colorectal cancer. N Engl J Med 369:1023–1034
10. Tabernero J, Lenz HJ, Siena S et al (2015) Analysis of circulating DNA and protein biomarkers to predict the clinical activity of regorafenib and assess prognosis in patients with metastatic colorectal cancer: a retrospective, exploratory analysis of the CORRECT trial. Lancet Oncol 16: 937-948.
11. Lubner MG, Stabo N, Lubner SJ et al (2015) CT textural analysis of hepatic metastatic colorectal cancer: pre-treatment tumour heterogeneity correlates with pathology and clinical outcomes. Abdom Imaging 40:2331–2337
12. Kawada K, Nakamoto Y, Kawada M et al (2012) Relationship between ^{18}F-fluorodeoxyglucose accumulation and KRAS/BRAF mutations in colorectal cancer. Clin Cancer Res 18:1696–1703
13. Miles KA, Ganeshan B, Rodriguez-Justo M et al (2014) Multifunctional imaging signature for V-KI-RAS2 Kirsten rat sarcoma viral oncogene homolog (KRAS) mutations in colorectal cancer. J Nucl Med 55:386–391
14. Kawada K, Toda K, Nakamoto Y et al (2015) Relationship between 18F-FDG PET/CT scans and KRAS mutations in metastatic colorectal cancer. J Nucl Med 56:1322–1327
15. Chen SW, Chiang HC, Chen WT et al (2014) Correlation between PET/CT parameters and KRAS expression in colorectal cancer. Clin Nucl Med 39:685–689
16. Lovinfosse P, Koopmansch B, Lambert F et al (2016) ^{18} F-FDG PET/CT imaging in rectal cancer: relationship with the RAS mutational status. Br J Radiol 89:20160212
17. Krikelis D, Skoura E, Kotoula V et al (2014) Lack of association between KRAS mutations and 18F-FDG PET/CT in Caucasian metastatic colorectal cancer patients. Anticancer Res 34:2571–2579
18. Huang YQ, Liang CH, He L et al (2016) Development and Validation of a Radiomics Nomogram for Preoperative Prediction of Lymph Node Metastasis in Colorectal Cancer. J Clin Oncol 34: 2157–2164
19. Nie K, Shi L, Chen Q et al (2016) Rectal cancer: assessment of neoadjuvant chemoradiation outcome based on radiomics of multiparametric MRI. Clin Cancer Res 22:5256–5264
20. Gillies RJ, Kinahan PE, Hricak H (2016) Radiomics: images are more than pictures, they are data. Radiology 278:563–577
21. Zhang B, Tian J, Dong D et al (2017) Radiomics features of multiparametric MRI as novel prognostic factors in advanced nasopharyngeal carcinoma. Clin Cancer Res 23:4259–4269
22. Coroller TP, Grossmann P, Hou Y et al (2015) CT-based radiomic signature predicts distant metastasis in lung adenocarcinoma. Radiother Oncol 114:345–350
23. Vallières M, Kay-Rivest E, Perrin LJ (2017) Radiomics strategies for risk assessment of tumour failure in head-and-neck cancer. Sci Rep 7:10117
24. Liu Z, Zhang XY, Shi YJ et al (2017) Radiomics analysis for evaluation of pathological complete response to neoadjuvant chemoradiotherapy in locally advanced rectal cancer. Clin Cancer Res. https://doi.org/10.1158/1078-0432.CCR-17-1038
25. Aerts HJ, Velazquez ER, Leijenaar RT et al (2014) Decoding tumour phenotype by noninvasive imaging using a quantitative radiomics approach. Nat Commun 5:4006
26. Boonstra K, Weersma RK, van Erpecum KJ, Rauws EA, Spanier BW, Poen AC (2013) Population-based epidemiology, malignancy risk, and outcomeof primary sclerosing cholangitis. Hepatology 58: 2045–2055
27. Reyes O, Morell C, Ventura S (2015) Scalable extensions of the ReliefF algorithm for weighting and selecting features on the multi-label learning context. Neurocomputing 161:168–182
28. Vandenberghe R, Nelissen N, Salmon E et al (2013) Binary classification of 18 F-flutemetamol PET using machine learning: comparison with visual reads and structural MRI. Neuroimage 64:517–525
29. Roffo G, Melzi S, Cristani M (2015) Infinite feature selection. Proceedings of the IEEE International Conference on Computer Vision 4202–4210
30. Liu S, Liu S, Ji C et al (2017) Application of CT texture analysis in predicting histopathological characteristics of gastric cancers. Eur Radiol. https://doi.org/10.1007/s00330-017-4881-1
31. Shiri I, Rahmim A, Ghaffarian P, Geramifar P, Abdollahi H, Bitarafan-Rajabi A (2017) The impact of image reconstruction settings on 18F-FDG PET radiomic features: multi-scanner phantom and patient studies. Eur Radiol. https://doi.org/10.1007/s00330-017-4859-z
32. Baldus SE, Schaefer KL, Engers R, Hartleb D, Stoecklein NH, Gabbert HE (2010) Prevalence and heterogeneity of KRAS, BRAF, and PIK3CA mutations in primary colorectal adenocarcinomas and their corresponding metastases. Clin Cancer Res 16: 790–799
33. Esteva A, Kuprel B, Novoa RA et al (2017) Dermatologist-level classification of skin cancer with deepneural networks. Nature 542: 115–118
34. Anthimopoulos M, Christodoulidis S, Ebner L, Christe A, Mougiakakou S (2016) Lung pattern classification for interstitial lung diseases using a deep convolutional neural network. IEEE Trans Med Imaging 35:1207–1216
35. Emblem KE, Pinho MC, Zöllner FG et al (2015) A generic support vector machine model for preoperative glioma survival associations. Radiology 275:228–234